Global Ocean Altimetry with GPS Reflections from TechDemoSat-1

Jake Mashburn, Penina Axelrad, Stephen Lowe, and Kristine Larson,

TechDemoSat-1 (TDS-1) is an experimental GNSS Reflections (GNSS-R) satellite launched in 2014. The GNSS-R receiver onboard performs real time navigation and generates delay-Doppler correlation maps for Earth reflected GPS L1 C/A ranging signals. This research investigates the performance of the TDS-1 data for ocean surface altimetry retreivals. The analysis includes consideration of the transmitter and receiver orbits, time tag corrections, models for ionospheric and tropospheric delays, zenith to nadir antenna baseline offsets, ocean and solid Earth tides, and a comparison with mean sea surface topography. An error budget is compiled to account for each error source and compared to the experimentally derived surface height retrievals. By analyzing data sets covering global ocean surfaces over +/- 60 deg latitude, the current performance of spaceborne GNSS-R altimetry is experimentally established. In comparison with mean sea surface topography, the surface height residuals are found to be 6.4 m, 1σ with a 1 sec integration time. A discussion of the factors limiting this performance is presented, with implications for future GNSS-R altimetry missions designed for observation of mesoscale ocean flows.

***Index Terms*—Altimetry, Error Analysis, Global Positioning System, Modeling, Reflectometry**

I. Introduction

ANALYSIS and flight experiments have demonstrated that transmissions from Global Navigation Satellite System (GNSS) satellites can be used as opportunistic signals for multi-static remote sensing of ocean, land, and ice surfaces around the globe. The application of GNSS Reflectometry (GNSS-R) to ocean altimetry was initially proposed by Martin-Neira almost twenty-five years ago [1], with more recent studies advancing the analysis of system requirements and expected performance [2], [3], [4], [5], [6], [7], [8], [9]. These studies explore the advantages of passive multi-static GNSS-R over active monostatic spaceborne altimetry. Specifically, they identify reductions in onboard power requirements, system complexity, and cost for a passive GNSS receiver as compared to an active radar instrument; and increases in coverage made possible by simultaneous tracking of reflected signals from multiple GNSS satellites. It has been shown in recent simulations by Li et al. (2016), that an optimized spaceborne GNSS-R altimetry platform could produce scientifically valuable results for mesoscale oceanography. This requires spatial resolution on the order of tens of kilometers, with sub-meter height resolution [9], [10].

Past GNSS-R experiments have largely focused on land based and airborne receiver experiments demonstrating novel methodologies for applications such as altimetry, tide monitoring, soil moisture, sea surface roughness and wind speed [5], [11], [12], [13], [14], [3]. Space-based experimentation has been limited to fortuitous circumstances [15] and a few technology demonstration missions [16], [17], [18], [19], [20]. With the December 2016 launch of the 8-satellite CYGNSS constellation, a GNSS-R science mission designed to measure ocean surface wind speeds, there is also growing interest in assessing the capability of reflected GNSS signals for ocean altimetry from space. While dedicated experiments to demonstrate space-based GNSS-R altimetry are actively being planned [2], [21], such a platform does not currently exist. Further, performance analysis of code-based altimetry from space, especially with flight data, has been very limited in geographic scope, completeness of the path delay model, and retracking methods analysis. One recent example is an early analysis of TechDemoSat data for use in GNSS-R altimetry by Clarizia et al. [19].

Our objective is to more fully establish the current level of spaceborne GNSS-R altimetry performance based on flight data from a GPS-R technology demonstration not specifically designed for this purpose. We use data from TDS to examine open ocean measurements from around the globe at all times of day, and incorporate corrections for common propagation effects and dynamic surface topography. This methodology maximizes the amount of data used from each collection period, generalizes the retrieval of surface height measurements to all open ocean points, and yields the most precise experimental retrievals to date.

Taking advantage of publicly available GPS-R data sets from the TechDemoSat-1 (TDS-1) mission, a precursor to CYGNSS also developed by Surrey Satellite Technology Ltd [17], [18], we characterize the

J. Mashburn, P. Axelrad, and K. Larson are with the Department of Aerospace Engineering Sciences, University of Colorado, Boulder, CO, 80302 USA e-mail: jake.mashburn@colorado.edu.

S. Lowe is with the Jet Propulsion Laboratory, California Institute of Technology, Pasadena, CA.

Manuscript received August 1, 2017; revised November 16, 2017.

performance of GPS-R ocean altimetry using GPS L1 C/A code measurements. An error budget detailing the known error sources is compiled and compared with experimentally derived results. In doing so, we present the first global analysis of spaceborne GNSS-R ocean altimetry and describe practical techniques for correcting the effects of ionospheric and tropospheric delays, receiver/transmitter orbital motion, and the receiving antenna geometry. The following sections describe the TDS-1 mission, instrumentation, data sets, and results from sea surface height retrievals compared to models accounting for geoid topography, ionospheric and tropospheric delays, and precise reflection geometries. The limitations and issues encountered with these data are discussed, along with recommendations for future altimetry specific GNSS-R work.

II. Spaceborne GNSS-R with TechDemoSat TDS-1

The Surrey Satellite Technology Ltd (SSTL) TDS-1 spacecraft, carrying an SGR-ReSI instrument, was launched into a sun-synchronous orbit with 650 km altitude in July 2014 [18]. From this vantage point, TDS-1 can view the entire globe, pole to pole, while remaining continuously within view of the medium Earth orbit (MEO) GNSS constellations. As TDS-1 orbits below the GPS constellation, specular reflection ray paths connecting the transmitter, surface, and receiver, track along the surface. Fig. 1 illustrates the spaceborne reflection geometry and the observed reflection ground track coverage of TDS-1 for the data sets used in this analysis. All of the reflection data analyzed here are taken from the MERRByS portal, www.merrbys.co.uk, where SSTL has made the TDS-1 measurements freely available to the international community [17].

The SGR-ReSI receiver was chosen to fly on TDS-1 as a technology demonstration in preparation for its use as the primary instrument for observation of ocean wind speeds on the CYGNSS mission [16]. Thus, the GNSS-R receiver system on TDS-1 has been optimized for ocean surface wind speed retrieval rather than altimetry. The resulting limitations and issues for altimetry include a relatively low-gain nadir pointing antenna; imprecise onboard positioning and timing with no recorded carrier phase data; tracking of only single-frequency, low-bandwidth signals, and an ambiguity in the reflection tracking point that prevents accurate retracking in post-processing. Despite these issues, which are discussed in detail in the following sections, the TDS-1 experiment does provide the most extensive spaceborne GPS-R data sets gathered to date, allowing a realistic, global assessment of on-orbit performance to be carried out.

For the analysis presented in this paper, data from two collection periods, RD17 and RD18, spanning four days and more than 100,000 reflection events in February 2015 are selected. Reflection retrievals from these data sets demonstrate consistently strong signal-to-noise ratios, with reflected signal path delays from which systematic effects can be effectively calibrated. The available data include measured delay-Doppler maps (DDMs) and synchronized metadata describing the reflection time, receiver clock corrections, and the computed receiver, transmitter, and reflection locations [22].

Unwin et al. describe the SGR-ReSI receiver and its implementation on TDS-1 [17], [18]. GNSS tracking on TDS-1 is limited to the GPS L1 C/A signal only for both positioning and reflection tracking. The satellite carries a standard ~ 4 dBi zenith-pointing RHCP antenna for direct signal tracking and a 13 dBi nadir-pointing LHCP antenna for reflection tracking. The SGR-ReSI has 28 tracking channels, with the ability to track 24 direct and 4 indirect signals [17].

Direct signals are tracked using a standard early-minus-late delay lock loop, from which pseudorange measurements are derived [23]. An onboard navigation processor forms point position and clock solutions from these observations every second. Based on the direct position solution and the Broadcast GPS satellite ephemerides, a computationally efficient geometric model is implemented onboard to predict the location and delay for a reflected signal from the Earth surface. An open-loop tracking algorithm is applied to the reflected signal, in which the signal received by TDS-1 nadir-pointed antenna is correlated against a locally generated model of the direct line-of-sight signal, offset by the expected delay and Doppler. The resulting correlation power is sampled in delay and Doppler space to form a Delay-Doppler Map (DDM) as described in [24], [7], [18]. DDMs for highly specular reflections appear as simply attenuated and delayed versions of the direct signal. DDMs for reflections from a rough ocean surface exhibit the characteristic horse shoe shape shown in Fig. 2, [24].

III. Ocean Altimetry Retrieval Methods

The three key features of the DDM are its shape, amplitude, and time delay (or path delay when multiplied by the speed of light) relative to the direct signal. The observed shape and amplitude of the DDM correlation function are highly dependent on the reflecting surface roughness that determines the scattering area and thus spread of the waveform in delay; and the dielectric constant that determines the scattered power. Determining the time delay of the specular reflected signal with respect to the direct, allows retrieval of a relative surface height [24]. That excess path delay of the specular reflection ray with respect to the direct ray is determined by re-tracking the delay of the correlation

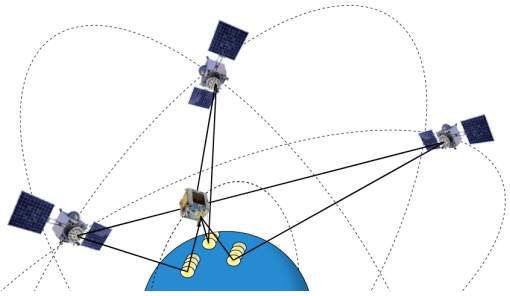

(a)

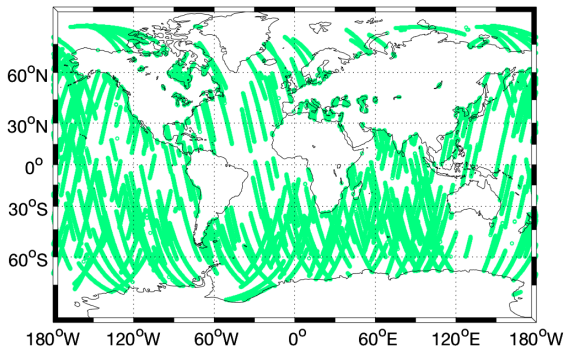

(b)

Fig. 1. (a) Cartoon of the GPS-R event geometry. As the transmitter (GPS) and receiver (TDS-1) orbit, the specular reflection points track along the surface. Multiple reflection events may occur simultaneously originating from different transmitters. (b) Global reflection ground track coverage from TDS-1 over four days from datasets RD17 and RD18 (available at www.merrbys.co.uk). About 100,000 reflection events are observed here. The data are masked to exclude land reflections.

function recorded in the DDM. The specular point delay is used as the track point, because it can be readily modeled and is less sensitive to roughness than the delay of the peak power or other possible track points on the waveform.

To assess the accuracy of GPS-R we compare the re-tracked/measured delay with a precise delay model. The measured delay anomaly with respect to our model is then given by

$$\Delta\delta = \delta_{measured} - \delta_{modeled}. \quad (1)$$

Delay anomaly (here in units of distance) is mapped into height anomaly from the modeled surface by

$$\Delta h = \frac{\Delta\delta}{2 \cdot cos(\theta)} \quad (2)$$

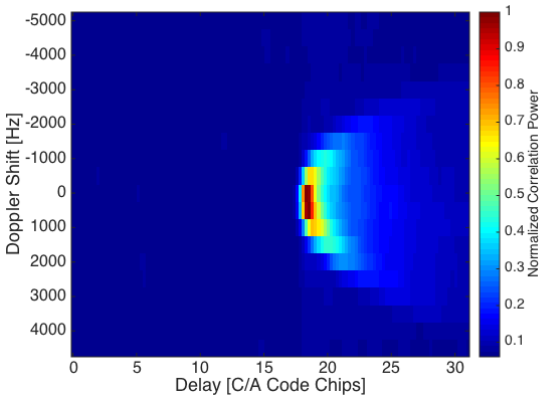

Fig. 2. An example delay-Doppler map (DDM) generated from tracking an ocean reflected signal. Correlation power is sub-divided into delay and Doppler bins to produce a DDM.

where θ is the reflection incidence angle. This trigonometric relation is derived from assuming that (a) the transmitter is far enough away that the incoming ray paths can be considered parallel, and (b) the reflecting surface is flat. While neither assumption is completely valid when considering the total excess path delay to a receiver in low Earth orbit, for the purpose of mapping range anomalies to height anomalies, the simplified mapping function is quite sufficient, introducing errors less than 1 mm in height.

Excess path delays are estimated across the entire globe using precise spacecraft orbits, mean sea surface topography, modeled atmospheric delays, and knowledge of TDS-1 antenna configuration. The following subsections detail the high fidelity reflection model, the operation of the TDS-1 SGR-ReSI open loop reflection tracking, the approach we used for waveform re-tracking, and the calibrations we performed with the TDS-1 data set.

A. *Reflection Modeling*

A high-fidelity model was assembled to simulate the true reflection geometry and signal propagation errors as accurately and precisely as possible. Each component of the model, the information source, and the estimated uncorrected and residual errors of that model component are listed in Table I. The high-fidelity model estimates the delay of the reflected signal using the receiver coordinates from the metadata with corrections for the antenna baseline, transmitter coordinates from IGS final orbits corrected for direct and reflected signal flight times [25], specular point coordinates computed on the DTU10 mean sea surface [26] with ocean and solid body tidal corrections [27], [28], [29], and modeled ionospheric [30], [31], [32] and tropospheric [33] delays. Electromagnetic bias is not included in the model

at this point because the magnitude, estimated to be $10 - 20$ cm [34], [35], is well below other current limitations of the observations and models.

TechDemoSat-1 uses GPS L1 C/A code pseudoranges for real time positioning. A navigation solution is calculated at 1 Hz, then decimated onboard and downlinked at 0.1 Hz. The 0.1 Hz points are interpolated in ground-processing back to the DDM measurement times [22]. There are, of course, limitations in the real time navigation such as the broadcast ephemeris, clock errors, ranging noise, uncorrected ionospheric delays, as well as interpolation artifacts in the published metadata. High-pass filtering the receiver orbit positions to remove long period systematic behaviors reveal that the point solution variability is $\sim$ 2.6 m in 3D position. The orbit reported in the metadata for TDS-1 has been used in the high fidelity reflection model - this is the best option since we do not have knowledge of the exact onboard solution used for positioning the reflection tracking delay offset, or high quality, raw pseudorange and phase observations that could be used to construct a more precise post-processed orbit solution for TDS-1.

The high precision, final GPS satellite orbit and clock products, estimated by the International GNSS Service (IGS) [25] are used in computing the high fidelity model. The broadcast ephemerides, which are used in the onboard real time navigation of TDS-1, are estimated to be accurate to $\sim$ 1 m while the final orbits are estimated to be accurate to $\sim$ 3 cm in position [36]. Corrections to the location of the transmitter for both the direct and reflected signals time of flight are accounted for, in order to accurately estimate the geometry of the observation. These corrections to the transmitter position result in a $\leq$ 20 cm difference in the reflected signal delay delay.

The reference used for the reflecting surface is the DTU10 mean sea surface, a 2 arc-minute resolution gridded mean ocean topography map from the Danish Technical University [26]. Tidal corrections including ocean and load tides from the Global Ocean Tide 4.10 (*GOT4.10*) model and solid body tides[1] are superimposed on the reference surface.

Given this surface, and the time history of positions of the TDS-1 receiver and GPS transmitters, we implement an iterative approach developed by Wu, et al. (1997) to compute the expected location of the specular reflection point on the surface [38]. The iteration adjusts the reflection point until the incident and reflecting angles agree to within 0.001 deg tolerance. In real time, TDS-1 predicts the delay and Doppler offsets of the specular point with a computationally efficient quasi-spherical Earth model that approximates the WGS84 reference ellipsoid [22]. This onboard model yields a reflection position that is $<$ 15 m of delay and $<$ 250 Hz Doppler shift compared to the correct WGS84 ellipsoid position. The quasi-spherical modeling delay error is known and completely accounted for in our model. The Doppler error for the high elevation angle reflections considered here is typically much less than the 250 Hz upper limit and much less than the Doppler resolution of the DDM measurements. Therefore, the targeted Doppler bin is used for re-tracking as described in Section III-B.

Corrections for ionospheric and tropospheric delays are also required. High precision orbit determination and scientific observations with GPS always rely on dual frequency (L1 and L2) measurements to directly measure and remove ionospheric effects [39]. Unfortunately, TDS-1 and other low cost missions, tend to forgo the dual frequency capability, relying solely on single frequency L1 measurements. Ionospheric models and mapping algorithms have been developed to support such missions. We use the International Reference Ionosphere 2012 (IRI2012) [32] to model the vertical total electron content ($vTEC$) values at ionospheric pierce points associated with each of the three ray paths illustrated in Fig. 3, namely, the rays from the GPS transmitter to TDS-1 ($vTEC_3$), the GPS transmitter to the ground reflection point ($vTEC_1$), and the reflection point to the TDS-1 ($vTEC_2$).

The vTEC values estimated for the two pierce points on the reflected path are mapped to slant path delays with the mapping function

$$M_{1,2}(E) = \frac{1}{\sqrt{1 - \left(cos(E) \cdot \frac{R_E}{R_E + h}\right)^2}} \tag{3}$$

given by Equation 4.20 in Komjathy (1997) [31], where E is the elevation angle at the reflection point, R_E is the Earth's radius, and h is the ionospheric shell height chosen to be 400 km.

Correction of ionospheric delay on the direct signal from the GPS to the TDS-1 is performed using a method developed by Montenbruck et al. (2002) [30]. The TEC column value, $vTEC_3$ in Fig. 3, is computed from IRI2012 extending to its uppermost altitude limit of 2000 km. Then the mapping function given by Montenbruck et al. (2002) [30] is specifically formulated to compute slant path delays for low Earth orbiting spacecraft and is given by,

$$M_3(E_{IP}) = \frac{\alpha}{sin(E_{IP})} \tag{4}$$

where E_{IP} is the elevation angle of the line of sight path through the ionospheric pierce point, and α,

$$\alpha = \frac{e - exp(1 - exp(-z_{IP}))}{e - exp(1 - exp(h_0/H))}, \tag{5}$$

[1]The solid body codes are available from Dennis Milbert at http://geodesyworld.github.io/SOFTS/solid.htm.

TABLE I
MODEL COMPONENTS WITH EXPECTED RMS ERROR IF LEFT UNCORRECTED AND RESIDUAL ERRORS AFTER CORRECTION.

Name	Source	Uncorrected Magnitude	Residual Error 1σ
TDS-1 orbit error	Metadata	2.6 m position	2.6 m position
GPS orbit error	[36], [25]	1 m position	0.03 m position
DTU10 MSS topography	[26]	100 m height	0.1 m height
Quasi-spherical Earth	[22]	15 m delay	0 m
Ocean/Body Tides	[27], [28], [29]	2 m height	0.1 m
Ionosphere delay	[30], [31], [32], [37]	15 m delay	6 m delay
Troposphere delay	[33]	6 m delay	0.05 m delay
Antenna Baseline	Metadata	1 m delay	0.001 m delay

is a scaling factor for the ionospheric density above the receiver altitude, which depends on the receiver altitude, h_s, the shell height, h_0, and a scale height, H. The variable z_{IP} is solved for from

$$exp(1-exp(-z_{IP})) = \frac{1}{2}(e+exp(1-exp(-z_s)));$$
$$z_s = (h_s - h_0)/H. \tag{6}$$

The total group delay along the reflected and direct ray paths is then estimated from those slant TEC values by

$$\delta_{1,2,3} = M_{1,2,3} \cdot \frac{40.3 \times 10^{16} \cdot vTEC}{f_{L1}^2} \tag{7}$$

and the excess delay on the reflected signal is

$$\delta_{iono} = (\delta_1 + \delta_2) - \delta_3. \tag{8}$$

Tropospheric delays are accounted for using the UNB3m model from the University of New Brunswick [33]. UNB3m uses empirically derived average atmospheric parameters computed for a grid of latitudes and seasons, Saastamoinen zenith delays [40], and Niell mapping functions [41] to estimate delays. Because the GPS-R receiver is spaceborne, the tropospheric delays are highly concentrated below an altitude of 10 km, and we are working with transmitting satellites at elevation angles above 60 deg; tropospheric corrections are only applied to the downward and upward reflected signal paths below the receiver altitude. The UNB3m model is evaluated at the specular point latitude and doubled to account for the down and up-traveling paths. As modeled by UNB3m, the latitudinal change of the tropospheric propagation delay is less than 0.5 cm/deg, and the pierce points of each reflection path through the troposphere are approximately 10 km apart. Therefore, evaluating the model at two separate pierce points is deemed unnecessary.

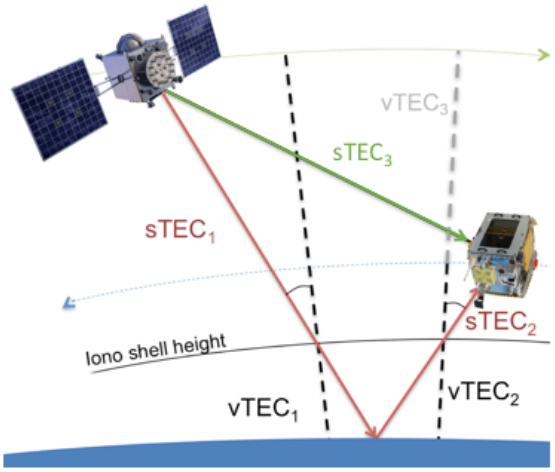

Fig. 3. The ionospheric delay effect is estimated on the reflected signal ray path. Vertical TEC ($vTEC$) columns at the up and down-traveling pierce points are evaluated from the IRI2012 model and mapped to slant angles. The summed slant TEC is used to estimate the excess delay effect.

When constructing the expected excess path delay for the reflected signal, one must also take into account the baseline offset between the zenith antenna used to track direct signals, and the nadir pointed antenna used to track reflections. To make this correction precisely, one would need information on the antenna installations, the effective phase centers of the two antennas, and the attitude or orientation of the satellite in its orbit. The coordinate of the antenna internal center on the face where it is mounted to the spacecraft body is given and TDS-1 is steered such that the body frame is aligned with the orbit local level (LVLH) frame [42], [22]. The body frame x-axis is aligned in the velocity direction, the body frame z-axis is aligned in the orbit radial

(local vertical) direction, and the body y-axis completes the right handed set. Thus, the antenna baseline vector, $\vec{b} = [-264.1,\ 399.1,\ -910.8]^T$ mm, given in the body frame is used to model the delay effect for a given incident signal by

$$\delta_{baseline} = (\mathbf{R}\ \vec{b}) \cdot \hat{e} \tag{9}$$

where $\mathbf{R}$ is the rotation matrix from the LVLH frame to the ECEF frame, $\vec{b}$ is the antenna baseline vector expressed in the body frame, and $\hat{e}$ is the line of sight direction to the GPS transmitter expressed in the ECEF frame. The rotation matrix $\mathbf{R}$ is computed from the basis vectors of the LVLH frame by

$$\mathbf{R} = \begin{bmatrix} \hat{v_1} & \hat{c_1} & \hat{r_1} \\ \hat{v_2} & \hat{c_2} & \hat{r_2} \\ \hat{v_3} & \hat{c_3} & \hat{r_3} \end{bmatrix} \tag{10}$$

where $\hat{v}$ is the spacecraft velocity direction (in-track), $\hat{r}$ is the orbit radial (local vertical) direction, and $\hat{c}$ completes the set in the cross-track direction, each written in the ECEF frame.

After accounting for each of the systematic delay effects described above, a bias of 8.8 m is observed between the measured excess delay and the high fidelity model. We attribute this bias to a combination of the re-tracking measurement bias and uncalibrated receiver hardware biases. It was found to be constant across all of the data sets analyzed here, thus, in the remaining results this fixed delay bias has been removed.

Finally, the statistics of the signal tracking errors due to noise were investigated through a Monte Carlo analysis. A subset of data ($N \approx 16,000$ waveforms) was chosen for this analysis that spanned the full range of latitudes, longitudes, and observed signal-to-noise-ratios (SNR's). For each correlation waveform the random noise on the samples was estimated by taking the standard deviation of the power of those samples at early delays, where no reflected signal power is present. Gaussian distributed random noise values with zero mean were generated and superimposed on the original waveform. This new realization of each measured waveform is made by

$$x_i[n] = x[n] + w[n] \tag{11}$$

where $x[n]$ are the original samples, $w[n]$ are the random noise values, and $x_i[n]$ are the samples that make up the ith waveform realization. For each measurement, 100 realizations were created and re-tracked as described in Section III-B. The change in re-track delay as a function of SNR is shown in Fig. 8. Here we define SNR as

$$SNR = \frac{P_{max} - P_{noise}}{P_{noise}}, \tag{12}$$

where P_{max} is the peak measured correlation power, and P_{noise} is the mean correlation noise power value.

B. DDM Re-tracking

A specular delay measurement is made from each 1-second incoherently integrated DDM. A slice along the delay axis of the DDM correlation function at the targeted Doppler shift creates a one-dimensional waveform that is used to re-track the specular reflection delay, see Fig. 4. The HALF re-tracking algorithm has been implemented similarly to our previous work with the Monterey Bay GNSS-R data set [11]. A point on the leading edge of the correlation waveform at 70% of the maximum correlation power is chosen as the re-tracking point. This HALF method, derived from standard monostatic radar techniques, is simple, computationally efficient, and results in a more precise delay measurement than other point tracking techniques [11], [5]. The small bias in tracking the 70% power point, as compared to the peak derivative point, has been removed as discussed in the previous section.

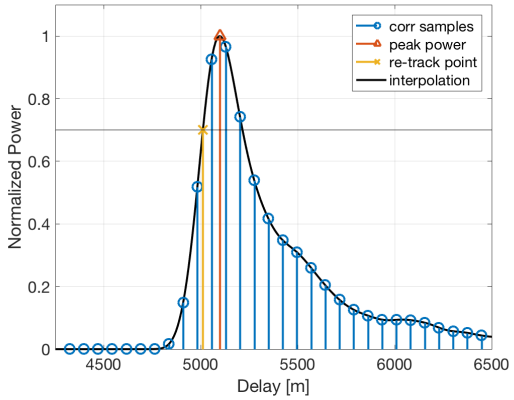

Fig. 4. An example of the correlation function re-tracking. First, the noise floor is determined by the average correlation value of the first 20 samples (not shown) and removed. The correlation waveform is then normalized by the peak power and the 70% tracking point is determined.

Tracking a specific point on the correlation waveform requires interpolation between samples. To do this, the noise floor is first computed by averaging correlation values of the first 20 samples where no signal is expected to be present, and then subtracted from the correlation measurements. A Whittaker-Shannon interpolation of the adjusted correlation measurements is used to precisely determine the desired points, as follows,

$$x(\delta) = \sum_{n=-\infty}^{\infty} x[n] \cdot sinc\left(\frac{\delta - nd}{d}\right) \tag{13}$$

where $x[n]$ are the normalized correlation samples after the noise floor has been removed, δ is continuous

delay, and d is again the sampling period. Newton's method is used to first locate the peak power point on the waveform and then the 70% re-track point.

C. On-board Delay Calculation and DDM Correlator Positioning

The TDS-1 flight software employs open loop tracking to position a bank of correlators in delay and Doppler space to capture the surface reflected signal [22]. The open loop tracking process is based on the quasi-spherical Earth model described previously and uses the WGS84 Earth-fixed positions and velocities of the receiver (TDS-1) and transmitter (GPS) taken from the real-time 1 Hz navigation solution. Delay and Doppler offsets from the closed loop direct signal tracking are computed and used to position the DDM correlation window. The received signal is then correlated against a locally generated replica of the direct signal that comes out of the closed loop direct signal tracking used for navigation.

Each DDM spans a limited range of the delay and Doppler space and generally includes only the reflected signal correlation function. Within the DDM window, the on-board reflection tracking point is specified by targeted delay (δ_{TP}) and Doppler (D_{TP}) values. The tracking point (δ_{TP}, D_{TP}) for a given DDM is referenced to the zero delay and zero Doppler of the correlation window (first row, center column of the DDM). Fig. 5 illustrates the measured re-tracking point and on-board predicted tracking point on an example DDM. The TDS documentation does not provide information about the direct signal tracking or the complete reflected signal delay-Doppler offsets. Because the DDM tracking point is provided as an offset from the target pixel, we must reconstruct the flight software reflection model in post processing to retrieve the full excess path delay. Therefore, the delay anomaly equation (1) is modified to become

$$\begin{aligned}\Delta\delta &= \Delta\delta_{measured} - \Delta\delta_{modeled} \\ &= (\delta_{re-track} - \delta_{TP}) \\ &- (\delta_{HiFi} - \delta_{on-board} + \delta_{tropo} + \delta_{iono})\end{aligned} \tag{14}$$

where $\delta_{re-track}$ is the measured delay on the DDM, δ_{TP} is the on-board predicted delay on the DDM, δ_{HiFi} and $\delta_{on-board}$ represent the reflected signal excess path delays as computed by our high fidelity geometric model and the reconstruction of the on-board calculations respectively, and δ_{tropo} and δ_{iono} are corrections for neutral and charged atmospheric delays.

D. TDS-1 On-board Model Calibration

The altimetric observable quantity from the TDS-1 data set is the delay difference between the re-track point and the on-board predicted track point. This difference is the path delay error caused by the true surface topography, systematic signal delays (e.g. troposphere and ionosphere), and any errors in the TDS-1 data set. Three issues with the TDS-1 metadata and the on-board reflection model have been identified and are compensated for in our analysis by reconstructing and subtracting a $\delta_{on-board}$ adjustment in (14). The observed on-board model implementation issues are as follows.

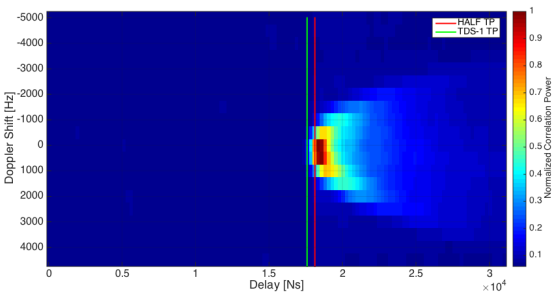

Fig. 5. An example DDM is shown with the open loop tracking point (δ_{TP} labeled TDS-1 TP) and re-track point ($\delta_{re-track}$ labeled HALF TP) indicated. Note that the delay axis begins at zero delay at the front of the DDM window.

First, there is a leap second error between the given UTC and GPS time stamps in the February 2015 metadata associated with each DDM. The UTC time stamps published in the metadata are computed on the ground by the SSTL analysis center, based on reported GPS times. An incorrect leap second adjustment has apparently been applied in the conversion. This error affects all of the time dependent parameters published in the metadata (e.g. receiver orbits, transmitter orbits, specular point locations, etc.), because those parameters are interpolated or re-evaluated in ground processing based on the UTC time stamp. It has been determined that the published GPS time stamps are correct, based on clear correlations between sharp changes in reflection power and known landmarks on the surface such as rivers [personal communication, Clara Chew 05/2016]. In our analysis all of the UTC times and affected model components have been corrected. The effect of this error is within ± 2 meters of delay.

Second, the delay anomalies in our analysis initially showed a strong linear dependence on the reflected signal range rate, which can be indicative of an error in the reported measurement time tags. We have observed what appears to be a consistent 0.1 second timing error between the TDS-1 open loop tracking model and the DDM measurements. A timing calibration correction has been imposed on the high-fidelity model to account for this. If left uncorrected, the effect of this range rate

dependent error would be quite large, on the order of ± 100 meters of delay.

Finally, what appears to be a geolocation mis-tagging error has been observed. When attempting to reconstruct the on-board delay model, $\delta_{on-board}$, for a given epoch, we were advised to use the specular point coordinate from the following index as given in (15) below, see supplementary material S4 of Chew et al. (2016) [14]. This result might indicate an indexing error in the TDS-1 onboard software used to predict the reflected signal delay. If uncorrected, the effect manifests itself in delay as a systematic latitude dependent error as if the predicted specular points are lagging. The effect of this error is large and a function of latitude, at ± 50 meters of delay.

$$\begin{aligned} \delta_{onboard} = &\|GPS_{xyz}(i) - SPT_{xyz}(i+1)\| \\ &+ \|TDS_{xyz}(i) - SPT_{xyz}(i+1)\| \\ &- \|GPS_{xyz}(i) - TDS_{xyz}(i)\| \end{aligned} \tag{15}$$

IV. Results

We measure the global agreement between GPS-R retrieved sea surface heights and the DTU10 (2 arc-minute) mean sea surface using TDS-1 datasets RD17 and RD18. Each of the observed DDMs is processed to extract the reflection SNR as defined in (12). Measurements with SNR of at least -5 dB are considered candidates for altimetric retrievals with expected tracking errors of $\sim$ 10 m, 1σ, as seen in Fig. 8(a). Observations are further limited to ocean regions where there is no possibility of ice coverage, specifically latitudes between N60 deg and S60 deg. These limits identified over 100,000 DDMs recorded in data sets RD17 and RD18, corresponding to 25% of the total collected, as viable for ocean altimetry. Further quality control filters removed any measurements with antenna gain $<$ 5 dB, delay residuals $>$ 250 m, and finally delay residual outliers greater than 4σ. Ninety-seven percent of the high SNR ocean reflections in the RD17 and RD18 datasets passed this quality screening. Fig. 6 presents the height retrieval results, where it is clear that the measured surface topography and the DTU10 model match on a global scale. Quantitative results are given in Table II and Fig. 7 with standard deviations of the delay and surface height residuals presented for 1, 10, and 60-second integration times. It should be noted that the delay and height anomaly standard deviations do not reduce by a factor of $\sqrt{N}$ as would be expected if the residuals were purely Gaussian white noise. This result indicates that there are some systematic effects remaining in our results, though they are hidden below the noise when considering 1 sec along-track integrations.

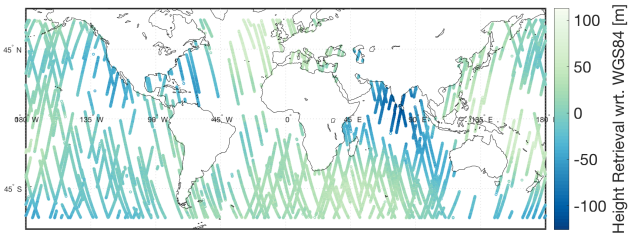

(a)

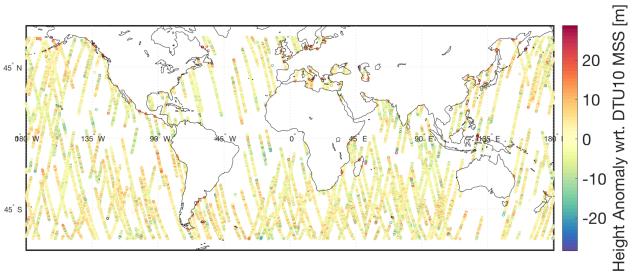

(b)

Fig. 6. (a) Measured ocean surface topography with respect to the WGS84 reference ellipsoid. (b) DTU10 mean sea surface model shown with respect to the WGS84 reference ellipsoid.

TABLE II
Residual delay and height anomalies from TDS-1 altimetry combining data sets RD17 and 18. The half re-tracking algorithm is used.

Integration Times	1σ **Delay Anomaly**	1σ **Height Anomaly**
1 s	11.9 m	6.4 m
10 s	5.5 m	2.9 m
60 s	4.6 m	2.6 m

TABLE III
Budget of residual measurement errors for a 1 second integration time.

Error Source	**Residual** 1σ
TDS-1 Orbit	2.6 m position
GPS Orbit	0.03 m position
Tides	0.1 m height
Ionosphere	6 m delay
Troposphere	0.05 m delay
Antenna Baseline	0.001 m delay
Tracking Error	10 m delay
RSS	12 m

The delay retrieval anomalies are seen to be well distributed in Fig. 7(a). Fig. 7(b) presents the delay anomalies plotted versus latitude, which shows no evidence of large geographic dependent effects visible in the residuals. For 1 second integrations the root-sum-square (RSS) of the tabulated residual errors (12 m, Table III) matches the observed precision of the delay anomaly (11.9 m, Table II).

The limiting factors in the accuracy and precision of these results are likely to be knowledge of the

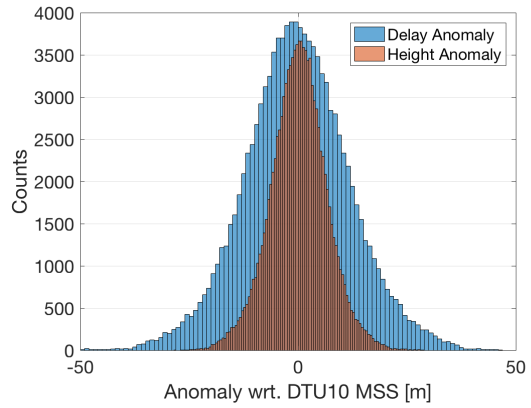

(a)

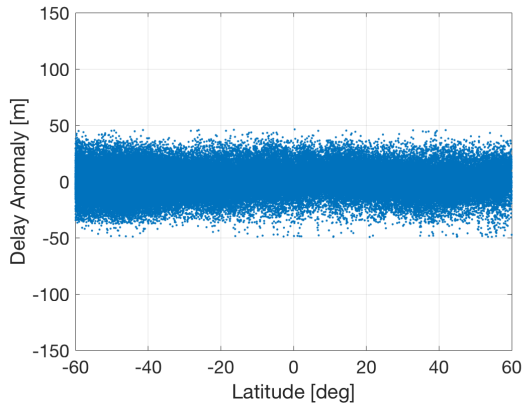

(b)

Fig. 7. (a) Histogram of the 1 second average delay anomaly residuals with respect to the tide corrected DTU10 MSS. (b) Delay anomaly residuals from the tide corrected DTU10 MSS shown against latitude.

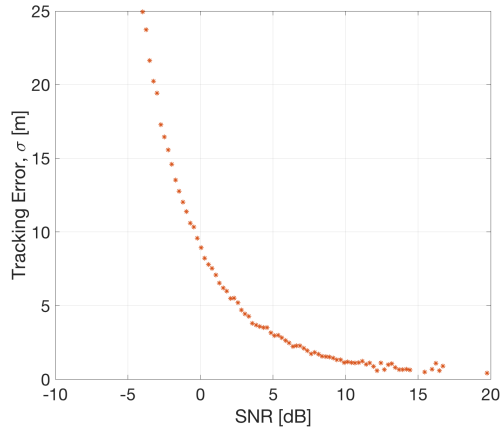

(a)

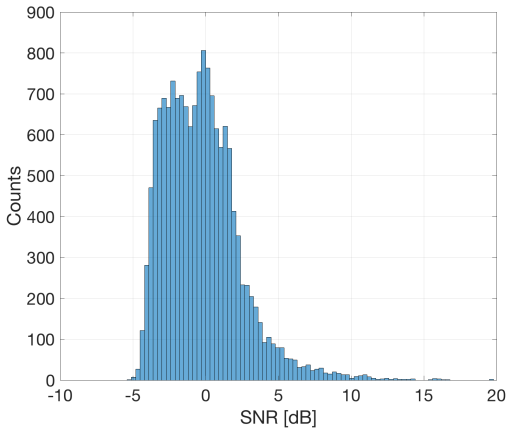

(b)

Fig. 8. (a) Estimated tracking error σ of the reflected signal as a function of signal to noise ratio. (b) A histogram of the observed signal to noise ratios of the reflected signals.

orbit and tracking noise. The residual orbit errors of the transmitter (0.03 m) and receiver (2.6 m) will of course not map directly into the path delay and are a likely source for some of the remaining systematic error effects. However, with the absence of a position error vector for each measurement, we assume a worst case scenario where the position error is included directly in the delay error budget, Table III. With this assumption we have a conservative estimate of the contribution from orbit precision.

Residual height errors from the tidal model are estimated to be about 0.1 m [28]. The *GOT4.10* model as it was used here includes ocean tides, and load tides. Solid body tides are also estimated from [29].

We also examined the impact of charged and neutral atmospheric effects. Because of the reliance on single frequency observations, we expected some limitations in performance due to the ionospheric effects. However, in comparing residuals for daytime and nighttime tracks, we do not see significant differences, with the daytime delay residuals having standard deviations of $\pm$12.7 m and nighttime tracks have standard deviation of $\pm$12.8 m in delay. The literature on ionospheric delay modeling suggests that the IRI-2012 model may have an error up to 40% in estimation of TEC [37]. A 40% error in the IRI TEC estimate results in $\sim$ 6 m of residual error in delay. Tropospheric models have been estimated to perform very well as compared to radiosonde profiles with a residual delay error of $\sim$ 5 cm [33].

The baseline offset between zenith and nadir looking antennas has been accounted for and the residual error is believed to be small. The typical attitude uncertainly of TDS-1 is $\sim$ 1 degree about each axis. This uncertainty in attitude yields an uncertainty in delay of about 1 mm.

Finally, the reflected signal tracking error as a function of correlation SNR has been analyzed. Fig. 8 illustrates the estimated tracking error of the reflected signal and

the distribution of observed correlation SNR values. It can be seen that the most often observed SNR, ~ 0 dB, corresponds to a tracking noise of ~ 10 meter standard deviation.

V. Summary and Conclusions

Our analysis of the TDS-1 data has established that spaceborne GNSS-R is capable of retrieving accurate global ocean altimetry, though as expected, the 1-sec measurement precision on this platform is not adequate for mesoscale oceanography. Based on the currently available data and models, the observed height retrieval precision is $\sigma_H = 6.4$ meters for 1 second integrations. The results presented here are based on a set of data not originally intended for altimetry, which brings up several challenges in the hardware and software implementation that have been compensated for as comprehensively as possible. Improvements to signal tracking would certainly be obtained through the use of a higher gain antenna and wider signal bandwidth. The use of dual frequency measurements would reduce the ionospheric error source to well below the required accuracy [39].

Aside from the limitations imposed by the TDS-1 receiver configuration, there are several propagation error model improvements that would yield much improved height retrieval precision. The most significant model improvements would come from better ionospheric corrections and precise receiver orbits. Improvements to these estimated orbits could likely be obtained in the future. Surrey Satellite Technology has indicated they may release the onboard orbit solutions or raw pseudorange measurements. One could then perform more precise orbit determination, directly improving the height retrievals. Finally, incorporating corrections for EM bias and other traditional ocean altimeter errors may give improvements on the order of 0.3 m [9], [34], [35], [43].

Even with an ideal GNSS-R configuration for altimetry, the achievable surface height precision is likely an order of magnitude larger than the current state-of-the-art nadir altimeters (e.g. JASON-2 [44]). Li, et al. suggest that such a system would require high gain antennas and utilize wide-band ranging codes and dual frequency signal tracking. Then the achievable height precision with GNSS-R is ~ 1 meter. However with appropriate spatial and temporal averaging of measurements from a small constellation of receivers, mesoscale ocean features may still be observable [9]. As more GNSS-R spacecraft become available (now TDS-1, CYGNSS, and SMAP [45]) the individual receiving systems are becoming increasingly capable. With a larger number of higher performance observing platforms, improvements to GNSS signal reflection models, and the incorporation of improved altimetric corrections the opportunities will grow for GNSS-R altimetry to provide useful oceanographic observations.

Acknowledgment

The work presented here was supported under JPL award #1538217. The authors would like to thank Dr. Clara Chew, Dr. Philip Jales, Dr. Dallas Masters, and Dr. Victor Zlotnicki for their valuable contributions. Dr. Chew helped us identify the source of systematic error sources encountered in the TDS-1 dataset. Dr. Jales was invaluable in initially understanding the TDS-1 operations and data sets. Dr. Masters provided us with specular point prediction code and tidal corrections to the mean sea surface. Finally, we would like to thank Dr. Zlotnicki for his helpful input. We appreciate Surrey Satellite Technologies Ltd. making their data from TechDemoSat-1 available to the public at www.merrbys.co.uk.

References

[1] M. Martin-Neira, "Passive reflectometry and interferometry system (PARIS). application to ocean altimetry," *ESA Journal (European Space Agency)*, vol. 17, no. 4, pp. 331 – 331, 1993.

[2] M. Martin-Neira, S. D'Addio, C. Buck, N. Floury, and R. Prieto-Cerdeira, "The PARIS ocean altimeter in-orbit demonstrator," *Geoscience and Remote Sensing, IEEE Transactions on*, vol. 49, no. 6, pp. 2209–2237, June 2011.

[3] V. U. Zavorotny and A. G. Voronovich, "Scattering of GPS Signals from the Ocean with Wind Remote Sensing Application," *IEEE Transactions on Geoscience and Remote Sensing*, vol. 38, no. 2, pp. 951–964, Mar 2000.

[4] S. D'Addio, M. Martin-Neira, and C. Buck, "End-to-end performance analysis of a PARIS in-orbit demostrator ocean altimeter," in *Geoscience and Remote Sensing Symposium (IGARSS), 2011 IEEE International*, July 2011, pp. 4387–4390.

[5] E. Cardellach, A. Rius, M. Martin-Neira, F. Fabra, O. Nogues-Correig, S. Ribo, J. Kainulainen, A. Camps, and S. D'Addio, "Consolidating the Precision of Interferometric GNSS-R Ocean Altimetry Using Airborne Experimental Data," *Geoscience and Remote Sensing, IEEE Transactions on*, vol. 52, no. 8, pp. 4992–5004, 2014.

[6] D. Masters, P. Axelrad, V. Zavorotny, S. Katzberg, and F. Lalezari, "A passive GPS bistatic radar altimeter for aircraft navigation," in *Proceedings of the 14th International Technical Meeting of the Satellite Division of The Institute of Navigation (ION GPS 2001)*, September 2001, pp. 2435–2445.

[7] S. Lowe, P. Kroger, G. Franklin, J. LaBrecque, J. Lerma, M. Lough, M. Marcin, R. Muellerschoen,

D. Spitzmesser, and L. Young, "A delay/doppler-mapping receiver system for GPS-reflection remote sensing," *Geoscience and Remote Sensing, IEEE Transactions on*, vol. 40, no. 5, pp. 1150–1163, May 2002.

[8] A. M. Semmling, V. Leister, J. Saynisch, F. Zus, S. Heise, and J. Wickert, "A Phase-Altimetric Simulator: Studying the Sensitivity of Earth-Reflected GNSS Signals to Ocean Topography," *IEEE Trans. Geoscience and Remote Sensing*, vol. 54, pp. 6791–6802, 2016.

[9] Z. Li, C. Zuffada, S. T. Lowe, T. Lee, and V. Zlotnicki, "Analysis of GNSS-R Altimetry for Mapping Ocean Mesoscale Sea Surface Heights Using High-Resolution Model Simulations," *IEEE Journal of Selected Topics in Applied Earth Observations and Remote Sensing*, vol. 9, no. 10, pp. 4631–4642, Oct 2016.

[10] C. G. Rapley, "Executive Summary of the Proceedings of the Consultative Meeting on Imaging Altimeter Requirements and Techniques," June 1990.

[11] J. Mashburn, P. Axelrad, S. T. Lowe, and K. M. Larson, "An Assessment of the Precision and Accuracy of Altimetry Retrievals for a Monterey Bay GNSS-R Experiment," *IEEE Journal of Selected Topics in Applied Earth Observations and Remote Sensing*, vol. PP, no. 99, pp. 1–9, 2016.

[12] E. Cardellach, F. Fabra, O. Nogues-Correig, S. Oliveras, S. Ribo, and A. Rius, "GNSS-R Ground-Based and Airborne Campaigns for Ocean, Land, Ice, and Snow Techniques: Application to the GOLD-RTR Data Sets," *Radio Sci.*, vol. 46, 2011.

[13] K. M. Larson, R. D. Ray, F. G. Nievinski, and J. T. Freymueller, "The Accidental Tide Gauge: A GPS Reflection Case Study From Kachemak Bay, Alaska," *IEEE Geoscience and Remote Sensing Letters*, vol. 10, no. 5, pp. 1200–1204, Sept 2013.

[14] C. Chew, R. Shah, C. Zuffada, G. Hajj, D. Masters, and A. J. Mannucci, "Demonstrating Soil Moisture Remote Sensing with Observations from the UK TechDemoSat-1 Satellite Mission," *Geophysical Research Letters*, vol. 43, no. 7, pp. 3317–3324, 2016, 2016GL068189. [Online]. Available: http://dx.doi.org/10.1002/2016GL068189

[15] S. T. Lowe, J. L. LaBrecque, C. Zuffada, L. J. Romans, L. E. Young, and G. A. Hajj, "First Spaceborne Observation of an Earth-Reflected GPS Signal," *Radio Science*, vol. 37, no. 1, pp. 7–1–7–28, 2002.

[16] C. S. Ruf, R. Atlas, P. S. Chang, M. P. Clarizia, J. L. Garrison, S. Gleason, S. J. Katzberg, Z. Jelenak, J. T. Johnson, S. J. Majumdar, A. Obrien, D. J. Posselt, A. J. Ridley, R. J. Rose, and V. U. Zavorotny, "New Ocean Winds Satellite Mission to Probe Hurricanes and Tropical Convection," *Bulletin of the American Meteorological Society*, pp. 385–395, 2016.

[17] M. Unwin, P. Blunt, R. De Vos Van Steenwijk, S. Duncan, G. Martin, and P. Jales, "GNSS Remote Sensing and Technology Demonstration on TechDemoSat-1," in *Proceedings of the 24th International Technical Meeting of The Satellite Division of the Institute of Navigation (ION GNSS 2011)*, Portland, OR, United states, 2011, pp. 2970 – 2975.

[18] M. Unwin, R. De Vos Van Steenwijk, C. Gommenginger, C. Mitchell, and S. Gao, "The SGR-ReSI - A New Generation of Space GNSS Receiver for Remote Sensing," in *Proceedings of the 24th International Technical Meeting of The Satellite Division of the Institute of Navigation (ION GNSS 2011)*, Portland, OR, United states, 2010, pp. 1061 – 1067.

[19] M. P. Clarizia, C. Ruf, P. Cipollini, and C. Zuffada, "First Spaceborne Observation of Sea Surface Height Using GPS-Reflectometry," *Geophysical Research Letters*, vol. 43, no. 2, pp. 767 – 774, 2016.

[20] M. Unwin, S. Gleason, and M. Brennan, "The Space GPS Reflectometry Experiment on the UK Disaster Monitoring Constellation Satellite," in *Proceedings of the 16th International Technical Meeting of the Satellite Division of The Institute of Navigation (ION GPS/GNSS 2003)*, September 2003, pp. 2656–2663.

[21] J. Wickert, E. Cardellach, M. Martn-Neira, J. Bandeiras, L. Bertino, O. B. Andersen, A. Camps, N. Catarino, B. Chapron, F. Fabra, N. Floury, G. Foti, C. Gommenginger, J. Hatton, P. Heg, A. Jggi, M. Kern, T. Lee, Z. Li, H. Park, N. Pierdicca, G. Ressler, A. Rius, J. Rosell, J. Saynisch, F. Soulat, C. K. Shum, M. Semmling, A. Sousa, J. Xie, and C. Zuffada, "GEROS-ISS: GNSS REflectometry, Radio Occultation, and Scatterometry Onboard the International Space Station," *IEEE Journal of Selected Topics in Applied Earth Observations and Remote Sensing*, vol. 9, no. 10, pp. 4552–4581, Oct 2016.

[22] P. Jales, *MERRByS Product Manual*, 2nd ed., Surrey Satellite Technology LTD, May 2016.

[23] P. Misra and P. Enge, "Global Positioning System: Signals, Measurements and Performance Second Edition," *Massachusetts: Ganga-Jamuna Press*, 2006.

[24] J. L. Garrison and S. J. Katzberg, "The Application of Reflected GPS Signals to Ocean Remote Sensing," *Remote Sensing of Environment*, vol. 73, no. 2, pp. 175 – 187, 2000.

[25] J. M. Dow, R. E. Neilan, and C. Rizos, "The International GNSS Service in a Changing Landscape of Global Navigation Satellite Systems," *Journal of Geodesy*, vol. 83, no. 3, pp. 191 – 198, 2009.

[26] O. B. Andersen, "The DTU10 Gravity Field and Mean Sea Surface," in *Second International Symposium of the Gravity Field of the Earth (IGFS2)*, 2010.

[27] R. D. Ray, "A Global Ocean Tide Model from TOPEX/POSEIDON Altimetry: GOT99.2," NASA, Goddard Space Flight Center: Greenbelt, MD, USA, Tech. Rep. NASA/TM-1999-209478, 1999.

[28] D. Stammer, R. D. Ray, O. B. Andersen, B. K. Arbic, W. Bosch, L. Carrre, Y. Cheng, D. S. Chinn, B. D. Dushaw, G. D. Egbert, S. Y. Erofeeva, H. S. Fok, J. A. M. Green, S. Griffiths, M. A. King, V. Lapin, F. G. Lemoine, S. B. Luthcke, F. Lyard, J. Morison, M. Mller, L. Padman, J. G. Richman, J. F. Shriver, C. K. Shum, E. Taguchi, and Y. Yi, "Accuracy assessment of global barotropic ocean tide models," *Reviews of Geophysics*, vol. 52, no. 3, pp. 243–282, 2014.

[29] D. D. McCarthy and G. Petit, "IERS Conventions 2003 (IERS Technical Note; 32)," Frankfurt am Main: Verlag des Bundesamts für Kartographie und Geodäsie, Tech. Rep., 2004.

[30] O. Montenbruck and E. Gill, "Ionospheric Correction for GPS Tracking of LEO Satellites," *Journal of Navigation*, vol. 55, no. 2, pp. 293 – 304, 2002/05.

[31] A. Komjathy, "Global Ionospheric Total Electron Content Mapping Using the Global Positioning System," Ph.D. dissertation, University of New Brunswick, 1997.

[32] D. Bilitza, "The International Reference Ionosphere Status 2013," *Advances in Space Research*, vol. 55, no. 8, pp. 1914 – 1927, 2015.

[33] R. Leandro, M. Santos, and R. B. Langley, "UNB Neutral Atmosphere Models: Development and Performance," in *Proceedings of the 2006 National Technical Meeting of The Institute of Navigation*, Monterey, CA, United states, 2006, pp. 564 – 573.

[34] A. Camps, H. Park, I. Sekulic, and J. M. Rius, "GNSS-R Altimetry Performance Analysis for the GEROS Experiment on Board the International Space Station," *Sensors*, vol. 17, no. 7, 2017.

[35] A. Ghavidel, D. Schiavulli, and A. Camps, "Numerical Computation of the Electromagnetic Bias in GNSS-R Altimetry," *IEEE Transactions on Geoscience and Remote Sensing*, vol. 54, no. 1, pp. 489–498, Jan 2016.

[36] IGS. (2016) IGS Products, GPS Satellite Ephemerides. [Online]. Available: http://www.igs.org/products/data

[37] S. Kumar, "Performance of IRI-2012 Model During a Deep Solar Minimum and a Maximum Year Over Global Equatorial Regions," *Journal of Geophysical Research: Space Physics*, vol. 121, no. 6, pp. 5664–5674, 2016.

[38] S.-C. Wu, T. Meehan, and L. Young, "Potential Use of GPS Signals as Ocean Altimetry Observables," in *Proceedings of the National Technical Meeting, Institute of Navigation*, Santa Monica, CA, USA, 1997, pp. 543 – 550.

[39] F. K. Brunner, "An Improved Model for Dual Frequency Ionospheric Correction of GPS Observations," *Manuscripta Geodetica*, vol. 16, pp. 205–214, 1991.

[40] J. L. Davis, T. A. Herring, I. I. Shapiro, A. E. E. Rogers, and G. Elgered, "Geodesy by Radio Interferometry: Effects of Atmospheric Modeling Errors on Estimates of Baseline Length," *Radio Science*, vol. 20, no. 6, pp. 1593–1607, 1985.

[41] A. E. Niell, "Global Mapping Functions for the Atmosphere Delay at Radio Wavelengths," *Journal of Geophysical Research: Solid Earth*, vol. 101, no. B2, pp. 3227–3246, 1996.

[42] P. Jales and M. Unwin, "Mission Description - GNSS Reflectometry on TDS-1 with the SGR-ReSI," Surrey Satellite Technology Limited, Tech. Rep., 2015.

[43] G. A. Hajj and C. Zuffada, "Theoretical description of a bistatic system for ocean altimetry using the GPS signal," *Radio Science*, vol. 38, no. 5, 2003.

[44] (2017) OSTM/Jason-2 Products Handbook. [Online]. Available: http://www.ospo.noaa.gov/Products/documents/OSTMJason-2Products_Handbook.pdf

[45] H. Carreno-Luengo, S. Lowe, C. Zuffada, S. Esterhuizen, and S. Oveisgharan, "Spaceborne GNSS-R from the SMAP Mission: First Assessment of Polarimetric Scatterometry over Land and Cryosphere," *Remote Sensing*, vol. 9, no. 4, 2017.

Jake Mashburn is a Ph.D. student in the Department of Aerospace Engineering Sciences at the University of Colorado.

Penina Axelrad is Professor and Chair of Aerospace Engineering Sciences at the University of Colorado Boulder. She has been involved in GPS related research since 1986. Dr. Axelrad is a Fellow of the ION and the AIAA, a former president of the IION, and a member of the National Space-Based PNT Advisory Board.

Stephen Lowe Stephen T. Lowe received a B.S. degrees in physics and in mathematics from the Colorado School of Mines, Golden, CO, USA, and a Ph.D. degree in high-energy particle physics from the Stanford University, Stanford, CA, USA. Since 1987, he worked with the Tracking Systems and Applications group, Jet Propulsion Laboratory, California Institute of Technology, Pasadena, CA, USA.

Kristine Larson is a Professor of Aerospace Engineering Sciences at the University of Colorado. Her current research focuses on GPS reflections.